Current Research (2021) Newfoundland and Labrador Department of Industry, Energy and Technology Geological Survey, Report 21-1, pages 27-47

REE-Y PATTERNS AND FLUID INCLUSION ANALYSIS OF FLUORITES FROM THE AGS FLUORITE DEPOSIT, ST. LAWRENCE, NEWFOUNDLAND

Z. Magyarosi and J. Conliffe
Mineral Deposits Section

ABSTRACT

The AGS fluorite deposit is hosted in sedimentary rocks of the Inlet Group and the St. Lawrence Granite (SLG) intruding them. Fluorite mineralization occurs in veins and is divided into early, main and late stages, which are further subdivided into 10 phases. In this study, trace-element analysis, including rare earth elements (REE) and Y, fluid inclusion analysis, and detailed observations from previous studies were combined to examine the evolution of the AGS fluorite deposit.

In the early stage, fluids were a mixture of magmatic fluids, meteoric water and basinal fluids. The REE-Y patterns indicate a strong influence of the SLG, consistent with fluorite mineralization originating from volatile exsolution of the cooling granite. In the main stage, enhanced circulation of fluids in the sedimentary rocks led to changes in the composition of the fluids, followed by changes in the REE-Y patterns. In the late stage, further changes in the REE-Y patterns are due to the fluids being increasingly buffered by the sedimentary rocks and addition of carbonates to the fluids. The last phase of fluorite mineralization is the result of remobilization of earlier phases. Fluorite precipitation was due to mixing of fluids in the early stage and possibly change in pH in the main and late stages.

INTRODUCTION

This study examines the rare earth elements (REE) and selected trace-element contents as well as fluid inclusion analysis of fluorites from the AGS fluorite deposit near St. Lawrence, Newfoundland, to understand some of the processes that led to the fluorite mineralization. REE have long been used for understanding and characterizing geological processes because, with the exception of Ce and Eu, the REE behave similarly to each other due to their analogous size and same charge, and changes from this behaviour (*e.g.*, anomalies, enrichment in heavy REE (HREE) or light REE (LREE)), are related to specific conditions and processes (Loges *et al.*, 2013). Previously, REE were more commonly applied to understanding igneous processes, but the use of REE in examining hydrothermal processes has been increasing (Schwinn and Markl, 2005; Loges *et al.*, 2013; Deng *et al.*, 2014; Coşanay *et al.*, 2017; Schlegel *et al.*, 2020; Haschke *et al.*, 2021). The REE signatures of hydrothermal minerals in conjunction with other methods, such as fluid inclusion analysis, are a powerful tool for understanding hydrothermal processes.

The REE-Y patterns of fluorite are ideal for studying hydrothermal processes because REE readily substitute for Ca in the fluorite structure (Bau and Dulski, 1995; Magotra *et al.*, 2017). In addition, fluorite is typically associated with several critical elements, including REE, Y, Nb and Zr. Yttrium is usually included with the REE in these studies, because it is considered a pseudo-lanthanide due to its similar size and the same charge as the lanthanides, and it behaves anomalously in F-rich systems (Bau and Dulski, 1995; Loges *et al.*, 2013). The processes affecting REE-Y concentrations in fluorite (Möller *et al.*, 1998) include:

- REE-Y content of the source rock(s);
- Chemical complexation of REE-Y in fluids;
- Changes during fluid migration (adsorption of REE-Y onto mineral surfaces along the pathways of fluids);
- Fractionation during fluorite precipitation (re-ordering of ions within freshly precipitated surface zone);
- Influence of crystal growth rate and flow rate; and
- Type of REE-Y substitution.

There have been a number of previous studies including trace-element and fluid inclusion analyses of fluorites from the St. Lawrence area. These studies were completed prior to the discovery of the AGS deposit in 2013. The only known fluorite occurrence in the AGS area at the time of these earlier studies was the Grebe's Nest occurrence, located in the western end of the AGS deposit, where green fluorite is the most common phase. Strong *et al.* (1984) analyzed fluorites from several veins, but it is not clear if any of the

samples were from the Grebe's Nest occurrence. In that study, the fluorite phases were separated and analyzed with XRF, and the analytical data included trace-element data from nine of the REE and Y, as well as fluid inclusion analysis from different fluorite phases (Strong *et al.*, 1984). Collins (1992) analyzed fluorites from several fluorite veins in the St. Lawrence area including one sample from the Grebe's Nest occurrence containing green and minor amounts of blue fluorites. Samples were separated by hand and REE were analyzed using inductively coupled plasma-mass spectrometry (ICP-MS). Fluid inclusion analysis was also conducted on a number of fluorite phases, and the fluid inclusions were related to trace-element composition of various fluorite phases (Collins, 1992). Gagnon *et al.* (2003) analyzed fluorites from four deposits in North America including St. Lawrence. The samples from St. Lawrence were from three veins, including the Grebe's Nest vein, but no sample description was provided for any of the samples and it is not clear which phases of fluorite mineralization were analyzed. The analytical method was *in-situ* laser ablation-inductively coupled plasma-mass spectrometry (LA-ICP-MS) and included 29 elements including REE and Y. Since the studies of Strong *et al.* (1984) and Collins (1992), several publications have examined the trace-element and REE-Y contents of fluorites (*e.g.*, Bau and Dulski, 1995; Möller *et al.*, 1998; Loges *et al.*, 2013; Deng *et al.*, 2014; Coşanay *et al.*, 2017; Schlegel *et al.*, 2020; Haschke *et al.*, 2021). It is now apparent that the REE-Y and trace-element concentrations show significant variation at every scale, therefore the previous studies were not detailed or comprehensive enough to account for all these variations.

GEOLOGICAL SETTING

REGIONAL GEOLOGY

Fluorite mineralization in the St. Lawrence area is associated with the St. Lawrence Granite (SLG), located on the Burin Peninsula in the Avalon Zone of the Appalachian Orogeny in Newfoundland (Figure 1). The Avalon Zone consists of fault-bounded blocks of mainly Neoproterozoic arc-related volcanic and sedimentary rocks, and minor calc-alkaline to alkaline granitoids (Lilly, 1966; Williams *et al.*, 1974; Williams, 1995; King, 1988; Myrow, 1995; O'Brien *et al.*, 1996; Skehan, 1997; Mills *et al.*, 2016; van Staal and Zagorevski, 2017; Figure 1). The rocks were subjected to the Neoproterozoic Avalonian Orogeny, resulting in folding, faulting, uplift and erosion, and they were subsequently covered by Cambrian–Early Ordovician platformal shales (Smith and Hiscott, 1984). Finally, the region was locally intruded by Late Devonian post-orogenic granites, including the SLG (O'Brien *et al.*, 1996). The metamorphic grade is generally low, ranging up to lower-greenschist facies (Papezik, 1974).

LOCAL GEOLOGY

In the St. Lawrence area, the Burin Group, composed of mainly mafic volcanic rocks having a tholeiitic signature (Strong *et al.*, 1976, 1978; O'Driscoll *et al.*, 2001), represents the oldest rocks (Figure 1; 765 +2.2/-1.8 Ma; Krogh *et al.*, 1988; 764.5 ± 2.1 Ma; Murphy *et al.*, 2008). The Marystown Group underlies much of the Burin Peninsula and is mostly composed of bimodal volcanic rocks (Strong *et al.*, 1976) dated at 576.8 ± 2.8 and 574.4 ± 2.5 Ma (Sparkes and Dunning, 2014). The Musgravetown Group overlies the Marystown Group (Strong *et al.*, 1978; Hiscott, 1981) and is composed of clastic sedimentary rocks. Elsewhere in the Avalon Zone, rhyolitic rocks from the Musgravetown Group have been dated at 570 +5/-3 Ma (O'Brien *et al.*, 1989), 605 ± 1.2, 592 ± 2.2 and 591.3 ± 1.6 Ma (Mills *et al.*, 2017). The Inlet Group is inferred to be Cambrian, based on fossil evidence; it overlies rocks of the Burin and Marystown groups and is composed of fine-grained clastic sedimentary rocks, locally containing abundant limestone nodules and minor limestone beds (Strong *et al.*, 1978). The Rocky Ridge Formation (RRF) forms a discontinuous sequence of sodic amphibole-bearing felsic volcanic rocks occurring as up to 0.5 km^2 size "rafts" and "slabs" in the SLG (Strong *et al.*, 1978; Figure 1). The mineralogy of the RRF is similar to the SLG, and it is interpreted as a volcanic equivalent of the granite. Intrusive rocks in the study area include the Mount Margaret Gabbro, Loughlins Hill Gabbro, Seal Cove Gabbro, Anchor Drogue Granodiorite, Grand Beach Complex and SLG (Strong *et al.*, 1978; Figure 1). The Grand Beach Complex yielded an age of 394 +6/-4 Ma and shows many similarities to the SLG (Krogh *et al.*, 1988; Kerr *et al.*, 1993a). The other intrusive complexes, except the SLG, have not yet been dated.

The St. Lawrence Granite

The SLG is one of the highly evolved Devonian granites in Newfoundland, which are typically associated with various types of mineralization including fluorite (Figure 1). It is a peralkaline to metaluminous granite having an average F content of 993 ppm ranging up to 8760 ppm. The SLG intruded at shallow levels and is composed of several phases based on variations in texture, mineralogy and geochemistry. The south lobe (S lobe) of the granite is the only exposed phase associated with known economic quantities of fluorite mineralization (Figure 1). The AGS deposit is partially hosted in the AGS porphyry, but is underlain by a main granitic phase that is either part of, or similar to, the S lobe of the SLG. The granite was dated with U–Pb in zircon and yielded 374 ± 2 Ma for the S lobe (Kerr *et al.*, 1993b) and 377.2 ± 1.3 Ma for the AGS porphyry (Magyarosi *et al.*, 2019b). The main minerals in the peralkaline S lobe are perthitic feldspar, quartz, sodic amphibole and aegirine.

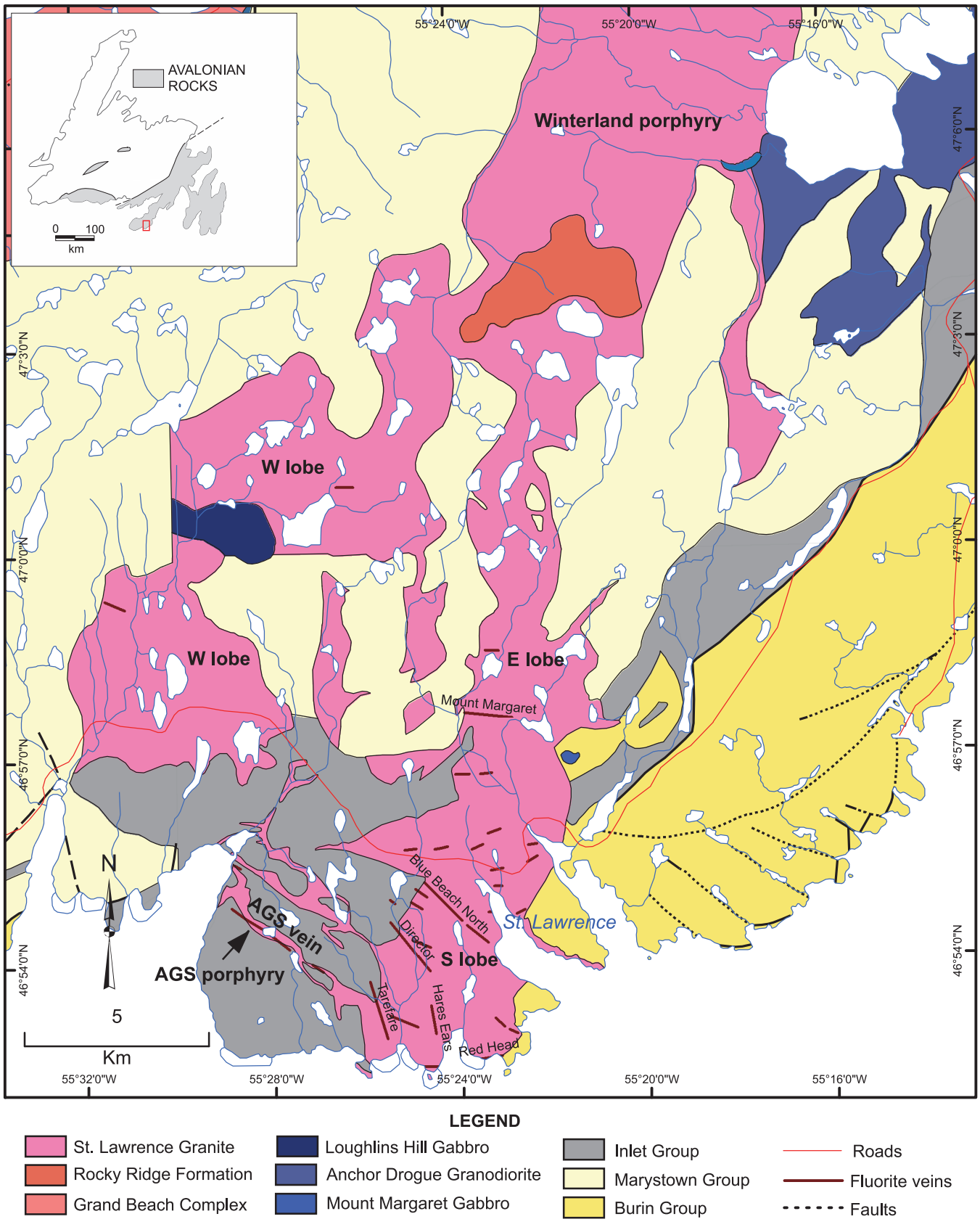

Figure 1. *Detailed geological map of the St. Lawrence area (after O'Brien* et al.*, 1976; Strong* et al.*, 1978).*

Accessory minerals include zircon, fluorite, calcite and several REE minerals. The AGS porphyry consists of mainly K-feldspar, quartz and plagioclase. The SLG is weakly to strongly altered. The strongest alteration is associated with the S lobe and around the fluorite veins, with sericite alteration dominating in the vicinity of the fluorite veins. Alteration in the S lobe includes albitization, the breakdown of arfvedsonite, magnetite altered to hematite and calcite replacing quartz, with the calcite postdating all previous types of alteration.

Fluorite Mineralization

The SLG is associated with more than 40 fluorite veins ranging in size from a few cm to 30 m in width, and up to 3 km in length (Figure 1; Reeves *et al.*, 2016). Fluorite mineralization is interpreted to originate from volatiles exsolving from the cooling granite. Most of the veins are hosted in faults and consist of several phases of fluorite, typically brecciated, with later phases cementing earlier phases and local extensional zones hosting high-grade mineralization (Van Alstine, 1948; Strong *et al.*, 1984; Magyarosi *et al.*, 2019b). Fluorite exhibits a variety of textures including breccia, stockwork veins, massive, crustiform, colloform, cockade and comb textures; most of which are indicative of their epithermal nature (Van Alstine, 1948; Magyarosi *et al.*, 2019b). Most of the fluorite veins identified are hosted in the SLG. The AGS deposit is the first deposit not entirely hosted in a main granitic phase (Magyarosi *et al.*, 2019b).

The AGS Fluorite Deposit

The AGS deposit is the most recently discovered, and currently the only producing fluorite mine in the St. Lawrence area. As defined, it is approximately 1.85 km long and consists of several veins that are up to 30 m in width and 700 m in length (Figure 1; Sparkes and Reeves, 2015; Reeves *et al.*, 2016). The deposit is hosted in sedimentary rocks of the Inlet Group and AGS porphyry sills intruding them, but the veins continue into a main phase of the SLG that was intersected by drilling between 250 and 300 m below the surface (Magyarosi *et al.*, 2019b). Fluorite mineralization is interpreted to originate mostly from the underlying granite, rather than the AGS porphyry. The deposit is located in a well-developed sinistral strike-slip fault.

Fluorite mineralization is divided into early, main and late stages, which are further subdivided into 10 phases (Table 1, Plate 1; Magyarosi *et al.*, 2019b). Fluorite is the main mineral in the veins and occurs in purple, yellow, green, blue, grey, white, red, pink and tan. Calcite is locally abundant, and occurs in variable amounts in most phases, with the amount of calcite generally increasing in the later phases. Quartz is typically associated with the earlier phases and the later phases. Sulphides include trace to minor amounts of sphalerite and galena, and trace amounts of pyrite and chalcopyrite.

Table 1. Paragenetic sequence

Stage	Phase		Description
Early stage	1	Barren breccia	Brecciated host rocks
	2	Purple fluorite	Stockwork, breccia with clasts of host rocks in purple fluorite matrix*
	3a	Fine-grained and yellow fluorite	Finely banded, fine-grained fluorite and/or coarse-grained yellow fluorite often alternating
	3b	Hematite–fluorite–quartz	Hematite with quartz and fluorite
Main stage	4	Reddish-grey fluorite	Massive, coarse-grained, grey, transparent fluorite, locally slightly reddish or pink
	5	Sulphides	Composed of sphalerite and minor galena
	6	Grey fluorite	Massive, grey fluorite with elongated crystals up to 20 cm in length
Late stage	7	Green fluorite	Predominantly green fluorite with minor white and blue fluorite
	8	Blue fluorite	Blue or clear cubic fluorite
	9a	Blastonite	Breccia composed of fragments of previous phases in a matrix composed of quartz and fine-grained fluorite
	9b	Late quartz	Quartz vein stockwork and vug filling
	10	Pyrite and chalcopyrite	Pyrite and chalcopyrite crystals in quartz lined vugs

*Variable amounts of calcite occur locally with fluorite in all phases.

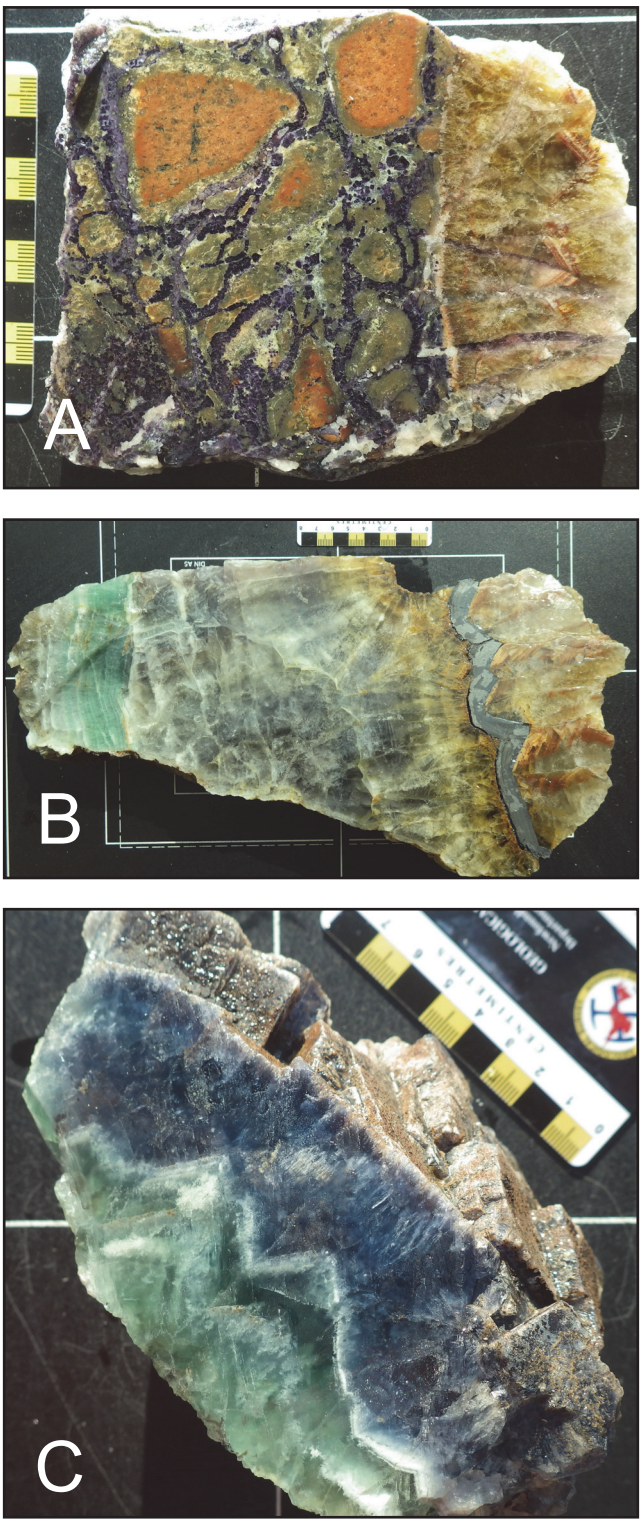

Plate 1. *Samples representing the three stages of fluorite mineralization. A) Stockwork purple fluorite with yellow fluorite from the early stage; B) Massive reddish-grey and grey fluorites separated by a band of sulphides composed of sphalerite and minor galena representing the main stage; C) Green and blue fluorites from the late stage.*

The early stage of fluorite mineralization consists of a strongly altered barren breccia; followed by purple fluorite forming stockwork veins or hydrothermal breccia composed of clasts of host rocks in a fluorite matrix (Table 1, Plate 1A). This is cut by banded, fine-grained fluorite and/or yellow coarse-grained fluorite, which is locally represented by fluorite intergrown with hematite and quartz. The main stage of mineralization consists of reddish-grey fluorite followed by grey fluorite forming elongated crystals, which are separated by a layer of fine-grained banded sulphides composed of sphalerite and minor galena (Table 1, Plate 1B). The late stage of mineralization consists of octahedral green fluorite interlayered with clear and rare blue fluorite, followed by blue or clear fluorite forming cubes, and a late quartz-rich fluorite phase with trace pyrite and chalcopyrite (Table 1, Plate 1C). For a more detailed description of the phases, *see* Magyarosi *et al.* (2019b).

ANALYTICAL METHODS

REE-Y AND SELECTED TRACE-ELEMENT ANALYSIS

The REE and selected trace-element contents of fluorites were analyzed using three methods including whole-rock, *in-situ* secondary ion mass spectrometer (SIMS), and LA-ICP-MS. The LA-ICP-MS data presented here is the most accepted and most common method for *in-situ* trace-element analysis of minerals (Gagnon *et al.*, 2003; Schwinn and Markl, 2005; Schlegel *et al.*, 2020; Haschke *et al.*, 2021). The LA-ICP-MS analysis includes more elements and is more representative of the whole grain than the SIMS analysis, because LA-ICP-MS analyzes a much larger area than SIMS, and balances the micro-scale heterogeneities within the fluorite grains. The use of LA-ICP-MS is also more accurate than the whole-rock analysis, because fluorites for whole-rock analysis were only roughly separated. Nevertheless, SIMS and whole-rock data provide a good tool to ensure the quality of the LA-ICP-MS data. The whole-rock analysis is in excellent agreement with the LA-ICP-MS data (Figure 2A). The SIMS data is also in very good agreement with the LA-ICP-MS data in most phases, except for the last two, where the SIMS data shows a greater variation, most likely indicating that these phases display significant small-scale variations not detected by the LA-ICP-MS (Figure 2B). This is consistent with Collins (1992) data that includes detailed analysis of only the last two phases from this area, also showing significant small-scale variations.

Whole-rock analysis was completed at the geochemical laboratory of the Geological Survey of Newfoundland and Labrador (GSNL) in St. John's. It included thirty-two samples of fluorite, representing each phase, roughly separated

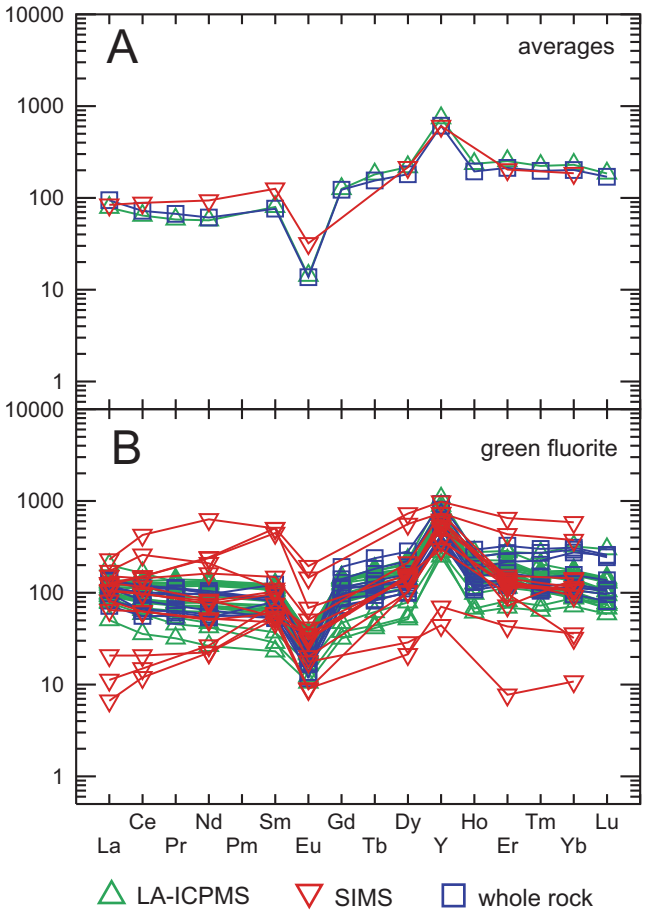

Figure 2. *Chondrite normalized (McDonough and Sun, 1995) plot of fluorites analyzed with three methods. A) Average fluorite REE-Y analysis in fluorite from all phases; B) Green fluorite analysis.*

from the host rocks and the other phases. Analytical and QA/QC procedures are described in Finch *et al.* (2018) and Magyarosi *et al.* (2019a). Whole-rock analysis of the S lobe of the granite, the AGS porphyry and the sedimentary rocks were also analyzed with the same method as the fluorites.

The SIMS analysis was completed using a Cameca IMS 4f SIMS instrument at the Memorial University MAF-IIC facility. The 17 by 17 mm wafers were prepared from 15 samples and mounted in epoxy inside one-inch aluminium rings. The samples were then polished to 1 µm using Tegramin-30 polisher by Struers (Pochereva, 2019). Samples were examined using a petrographic microscope and a FEI 650 Scanning Electron Microscope (SEM) at the Memorial University MAF-IIC facility to characterize mineral textures and compositions, and determine the areas to be analyzed. A thin layer of gold (approximately 300 Å) was applied to the samples using a sputter coater, preceding SIMS analysis. One to six spots were analyzed on each sample to account for zonal variations. The material removed from the sample at each spot was only about 3 μm^3 with a pit depth of a few µm (Pochereva, 2019; https://www.mun.ca/creait/MAF/SIMS_MAIN_cs.php). A borosilicate glass reference material (NIST 612) was used as a standard. Although the detection limits for most elements is below 1 ppm, the disadvantage of the SIMS is that the small amount of sample used for analysis may not be representative of the whole mineral grain due to local variations, as seen in the analysis of the green and blue fluorites.

The LA-ICP-MS measurements were completed on an ArF Excimer GeoLas laser ablation system (Coherent, Germany) coupled to an Element XR (Thermo Fisher, Germany). The laser operated at a frequency of 10 Hz with an energy density on the sample surface of 15 J/cm^2 and a spot size of 60 µm. Background was recorded before each measurement for 30 seconds and each spot was ablated for 40 seconds. The same 15 samples used for SIMS were also used for the LA-ICP-MS analysis. Two to four areas were selected on each sample and five spots were analyzed per each area. The analysis included all REE (except Pm), Na, Ca, Rb, Sr, Y, Zr and Ba. A borosilicate glass reference material (NIST 612) was used as primary standard while BCR-2G was used for quality control and the stoichiometric Ca concentration of fluorite was used as internal standard. The carrier gas flow was 1L/min He and the ICP-MS was tuned for high sensitivity while maintaining an ThO^+/Th^+ ratio of less than 0.3%.

FLUID INCLUSION ANALYSIS

Double polished fluid inclusion wafers (~100 µm thick) were prepared from samples representing the main fluorite phases. Petrographic descriptions of fluid inclusions were carried out using the Fluid Inclusion Assemblage (FIA) method, applying the criteria outlined in Goldstein and Reynolds (1994) and Goldstein (2003). Particular care was taken to determine which fluorite phase the inclusions were hosted in, and avoid FIA with signs of post-entrapment modifications (*e.g.*, decrepitation, leaking).

Microthermometric fluid inclusion analyses at Memorial University of Newfoundland used a Linkam THMSG600 heating–freezing stage mounted on an Olympus BX51 microscope. The heating–freezing stage was calibrated using synthetic H_2O and CO_2-H_2O fluid inclusion standards, with calibration measurements at melting point of CO_2 (-56.6°C), melting point of H_2O (0.0°C) and critical point of H_2O (374.1°C). Following procedures outlined by Shepherd *et al.* (1985), the temperature of homogenization (Th), eutectic melting temperature (Te), hydrohalite melting temperature (Tm (hh)) and final ice-melting temperature (Tm (ice)) were measured in two-phase (liquid + vapour) inclusions. The salts present in fluids were

estimated by comparing recorded eutectic temperatures with the known eutectic temperatures of common aqueous–salt systems. Salinities were calculated using Tm (ice) and the equation of Bodnar (1993), which calculates salinities as equivalent weight % NaCl (eq. wt. % NaCl). For inclusions where Tm (hh) and Tm (ice) were observed, fluid salinities (eq. wt. % NaCl + $CaCl_2$) and molar Na/(Ca + Na) ratios were calculated using the spreadsheet provided by Steele-MacInnis *et al.* (2011) for the H_2O-NaCl-$CaCl_2$ system.

RESULTS

REE-Y AND TRACE-ELEMENT CONCENTRATIONS

The REE-Y chondrite normalized patterns of the fluorites from the AGS deposit are typical of fluorite deposits associated with felsic igneous rocks (Magotra *et al.*, 2017). They are characterized by an enrichment in HREE compared to the LREE in most phases, with a negative Eu anomaly and a positive Y anomaly (Figures 3 and 4). The relative enrichment in HREE is shown as a combination of a weak positive slope from La to Lu, and the LREE displaying a convex pattern with Ce, Pr or Nd occupying the lowest point, and the HREE displaying a concave pattern with Er or Ho occupying the highest point, called the tetrad effect (Peppard *et al.*, 1969). The degree of HREE enrichment gradually increases through the paragenetic sequence of fluorite mineralization until the grey fluorite phase, followed by a decrease in the green fluorite and a reappearance in the blue fluorite (Figure 3, Table 1). The concentrations of both LREE and HREE are significantly lower in the blue fluorite, representing the last phase of fluorite mineralization (Figures 3 and 4). The size of the negative Eu anomaly is fairly consistent until the grey fluorite phase, but is gradually decreased in the last two phases (Figures 3 and 5). The REE-Y patterns of the granite and sedimentary rocks are plotted for comparison. Both the granite and the sedimentary rocks display a weak negative slope from La to Lu, indicative of LREE enrichment relative to HREE (Figures 3–5). The granite also displays a strong negative Eu anomaly and some samples display a weak positive or negative Ce anomaly and a very weak negative Y anomaly. The sedimentary rocks are also characterized by a negative slope from La to Lu, a weak negative Eu anomaly and one sample displays a weak positive Y anomaly. The size of the Eu anomaly is the largest in the granite, followed by the early and main stage fluorites, then the late stage fluorites, and it is the smallest in the sedimentary rocks (Figures 3 and 5).

The REE-Y patterns of all fluorites display a distinct positive Y anomaly (Figure 3). Calcite occurring with fluorite in some of the phases lacks the Y anomaly (Figure 6A). Figure 6B shows the AGS fluorites, the host granites and sedimentary rocks plotted on a Y/Ho *vs.* La/Ho diagram. Bau and Dulski (1995) suggested the use of this diagram to characterize the Y anomaly, because the ionic radius of Y^{3+} in an octahedral coordination is closest to Ho^{3+}, and the La/Ho ratio indicates changes in the behaviour of REE with increasing atomic number. The early fluorites (purple to reddish-grey phases) are situated along one line displaying a small range of Y/Ho and a much larger range of La/Ho. Most of the grey fluorites plot together in an area below the early phases and, with the exception of a few samples, do not show any significant variation in La/Ho or Y/Ho. Most of the green fluorites plot above the earlier phases with higher Y/Ho, with a few samples scattered below. Blue fluorites display a weak negative slope plotting above earlier phases.

The AGS fluorites were also plotted on a Tb/Ca *vs.* Tb/La diagram to examine crystallization environments and processes (Figure 7; *e.g.*, Möller *et al.*, 1976, 1998). According to Möller *et al.* (*op. cit.*), the Tb/La reflects changes due to fractionation (LREE *vs.* HREE), and the Tb /Ca ratio represents changes in the "chemical environment", which are not related to fractionation (*e.g.*, fluid mixing). The "sedimentary" field indicates fluorite formed in carbonates that were metasomatically altered by F-rich fluids. Within one phase, lower points represent early stages of crystallization, and upper points represent late crystallization (Möller *et al.*, 1976). Almost all fluorites from the AGS deposit plot in the hydrothermal field. Most of the fluorites also plot sub-parallel to a line indicative of primary crystallization. However, the blue fluorites, representing the last phase, plot along a secondary crystallization trend, suggesting that this phase formed as a result of remobilization of earlier fluorites.

Sodium has a positive correlation with the total REE-Y content in some of the phases, but the slope of this correlation is different in the individual phases (Figure 8A). Sodium also has a positive correlation with Sr (Figure 8B). The Zr content of fluorites in some phases is below or very close to the detection limit, but in the purple, yellow, green and blue phases, the Zr content ranges up to approximately 250 ppm (Figure 8C). The Zr content does not correlate with any other analyzed element.

FLUID INCLUSION ANALYSIS

Fluid inclusions were analyzed in six samples from the AGS fluorite deposit, which included fluorite phases from the main stage (grey and reddish-grey fluorite) and the late stage (green and blue fluorite). These data have been combined with fluid inclusion data from the early (purple, yellow and hematitic fluorite) and the late stages (green and blue fluorite) previously reported (Magyarosi *et al.*, 2019b),

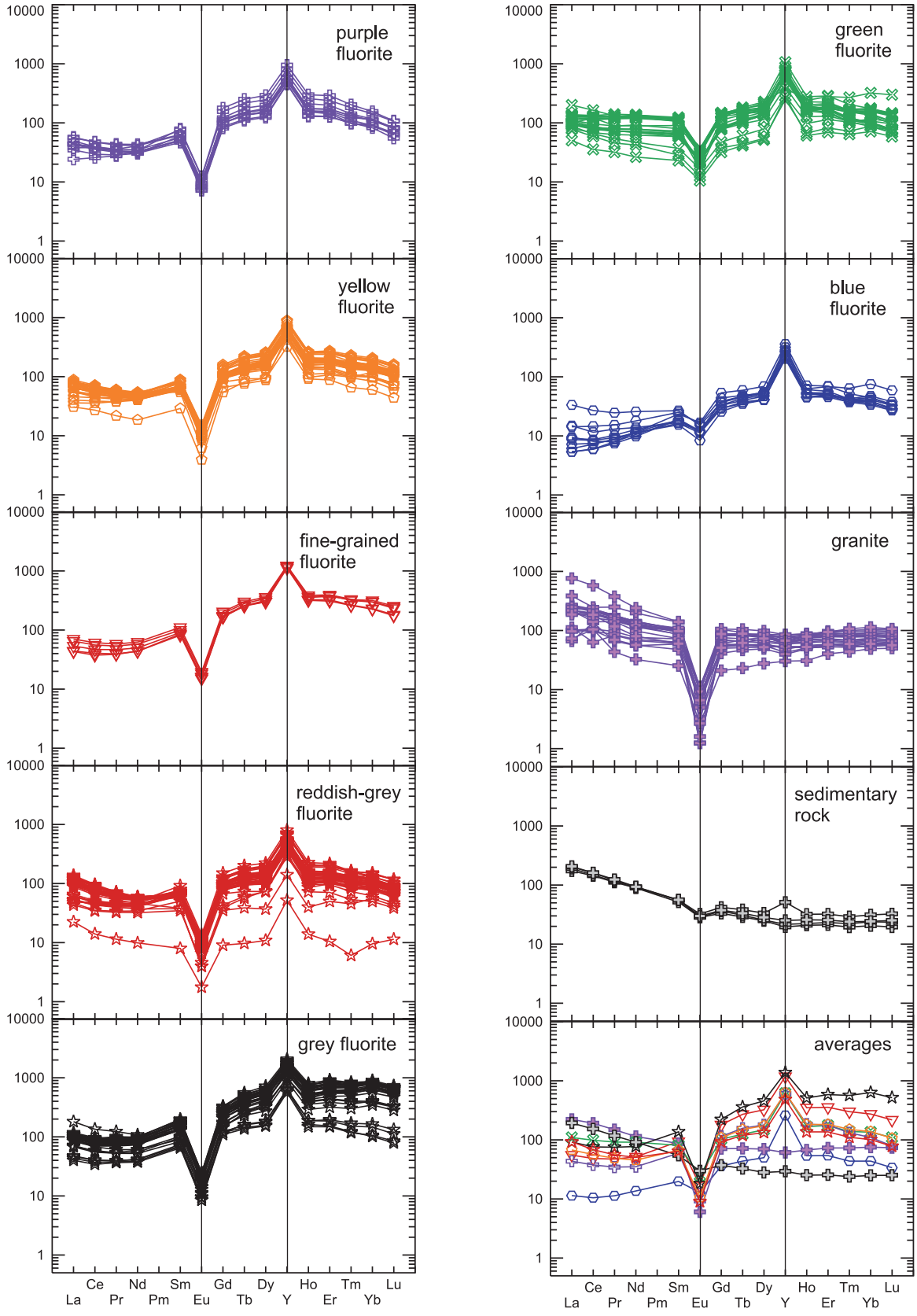

Figure 3. *Chondrite normalized (McDonough and Sun, 1995) REE-Y analysis of fluorites from each mineralization phase, the granites, and the sedimentary rocks.*

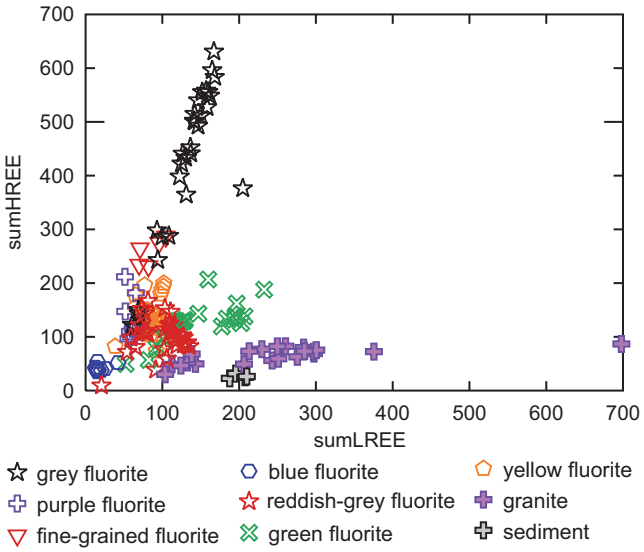

Figure 4. *Total HREE* vs. *total LREE plot of fluorites and host rocks.*

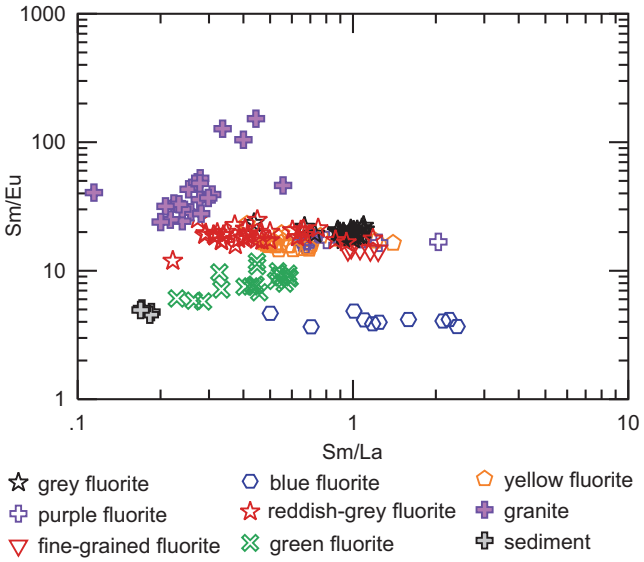

Figure 5. *Sm/Eu* vs. *Sm/La plot of fluorites and host rocks showing the degree of Eu anomaly.*

together covering all phases of fluorite mineralization at the AGS deposit.

Samples with fluorite from the early stage of mineralization are brecciated, with some primary FIA occurring with growth zones that are commonly crosscut by numerous trails of secondary FIA. In contrast, fluorite from the main and late stages are generally clear and inclusions occur in growth zones or as clusters of large inclusions (*i.e.*, primary FIA). Two-phase (liquid + vapour), liquid-rich fluid inclusions with ~5–10 % vapour dominate, but some three phase (liquid + vapour + solid) are also occasionally observed. The

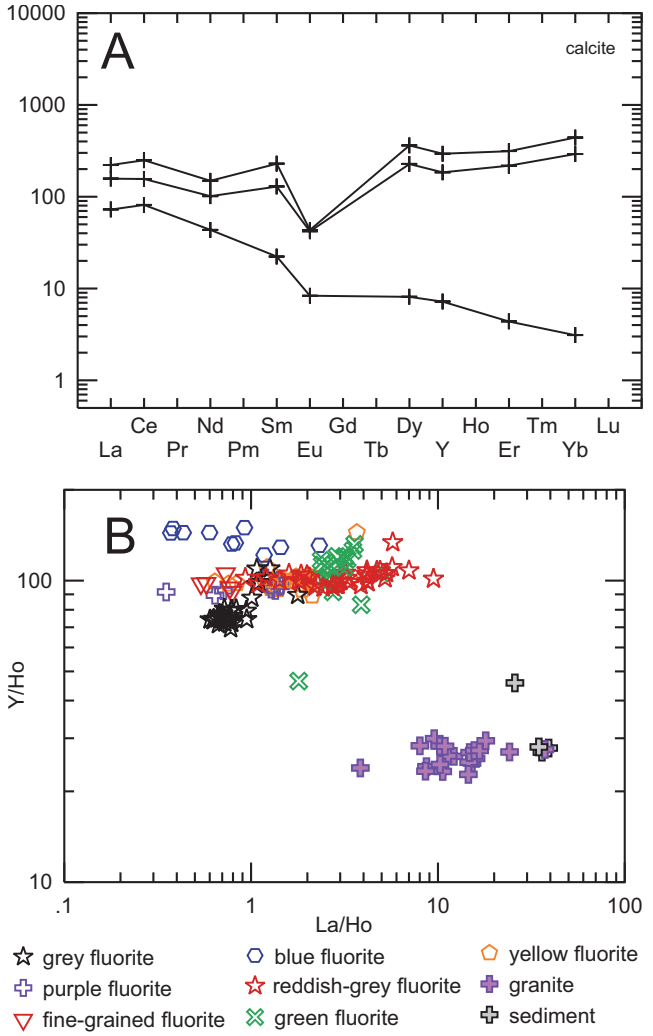

Figure 6. *A) Chondrite normalized (McDonough and Sun, 1995) analysis of calcite analyzed with SIMS; B) Y/Ho* vs. *La/Ho plot (after Bau and Dulski, 1995) of fluorites and host rocks showing the degree of Y anomaly.*

solid phases are variable, ranging from hematite inclusions (Plate 2A) to unidentified cubic phases (possibly fluorite; Plate 2B). The presence or absence of various solid inclusions is highly variable within the same FIA, and therefore solid inclusions are interpreted to represent accidently trapped solids rather than daughter crystals precipitated from the fluids.

Fluid inclusions are subdivided into two main types based on their characteristics, as determined during fluid inclusion microthermometry (Table 2). Type-1 inclusions are hosted in early-stage fluorite phases only. They occur in primary FIA (Plate 2C), and likely represent the fluids present during the precipitation of these early fluorite phases. Microthermometric measurements were obtained from 63 Type-1 inclusions in 17 FIA. Upon cooling to -120°C, these

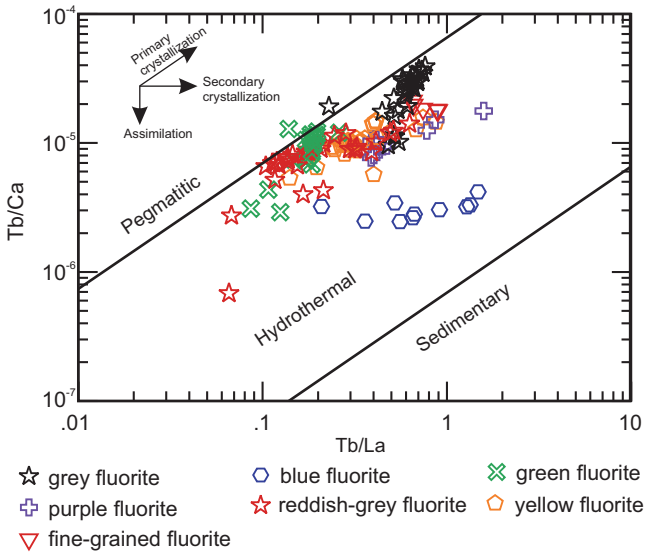

Figure 7. *Tb/Ca* vs. *Tb/La plot of fluorites (after Möller* et al.*, 1976, 1998). The diagram in the top left corner represents trends of fluorite mineralization in different crystallization environments and processes.*

inclusions freeze at between -70 and -80°C. First melting occurred close to the eutectic temperature of the H_2O-NaCl-$CaCl_2$ system (-52°C). Tm (hh) occurred prior to ice-melting temperatures between -41.2 and -24.2°C and final ice-melting temperatures are between -28.2 and -6.3°C (Table 2, Figure 9). These values indicate a wide range of salinities, and where Tm (hh) and Tm (ice) were observed in the same inclusions, salinities of 10.2 to 24.6 eq. wt. % NaCl+$CaCl_2$ were calculated with the Na/(Na + Ca) ratio ranging from 0.10 to 0.65. For inclusions where only Tm (ice) was observed, calculated salinities range from 9.6 to 27.5 eq. wt. % NaCl. Upon further heating, total homogenization to the liquid phase in Type-1 inclusions occurred between 89.3 and 159.6°C (mean = 120.5°C, standard deviation = 19.7°C), with temperatures in individual FIA varying by ± 5°C (Table 2, Figure 10).

Type-2 inclusions have been observed in all fluorite stages. In early-stage fluorites, Type-2 inclusions occur in trails of secondary FIA (Plate 2D), or in primary FIA in heavily brecciated samples where the fluorite may have undergone recrystallization by later fluids. In main- and late-stage fluorites, Type-2 inclusions occur in primary FIA away from secondary trails (Plate 2E, F). In total, microthermometric measurements were obtained from 189 Type-2 inclusions in 52 FIA. Type-2 inclusions freeze between -45 and -55°C, with no other phase changes observed during subsequent freezing to -150°C. Apparent first melting was observed between -44.5 and -33.1°C, but this may represent metastable phase transitions, which reduce the stability field of ice to lower temperatures (Bakker and Baumgartner,

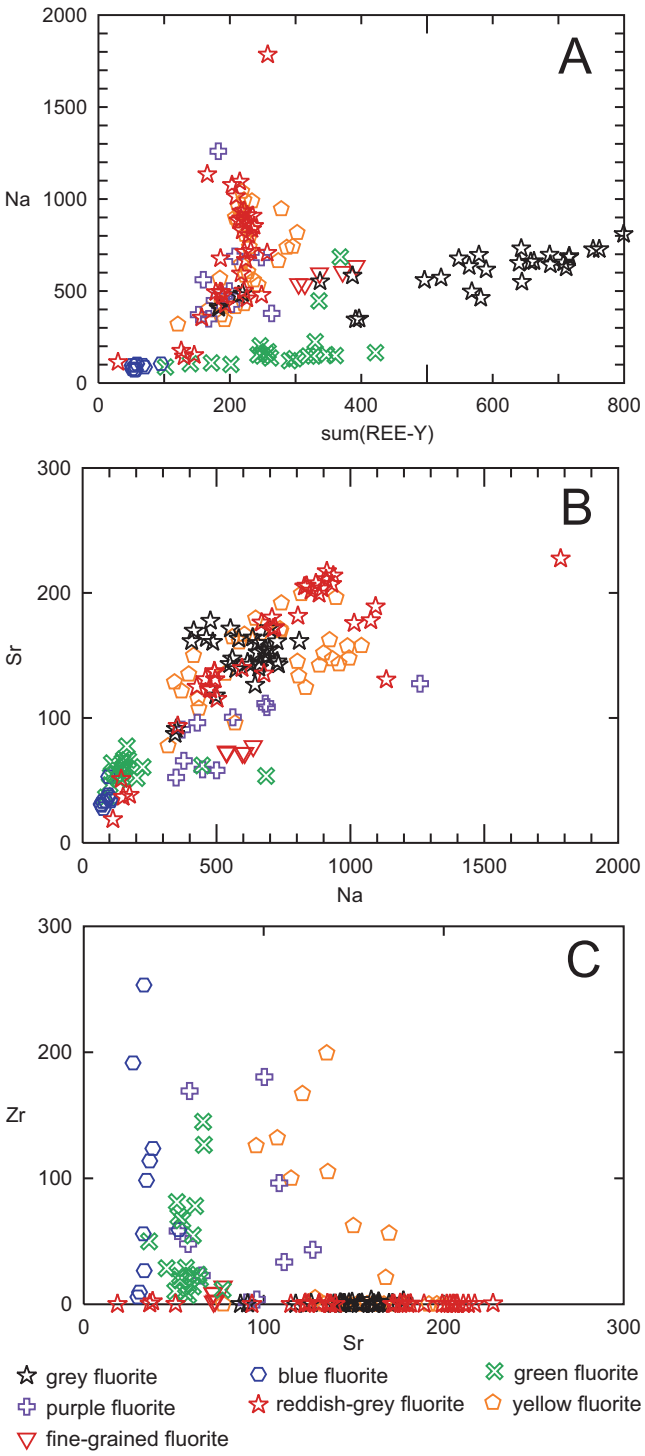

Figure 8. *Binary plots of trace element compositions of fluorites. A) Na* vs. *total REE-Y; B) Sr* vs. *Na; C) Zr* vs. *Sr.*

2012). However, sequential freezing and heating of Type-2 inclusions caused nucleation of all solid phases (*e.g.*, hydrohalite) and permitted measurement of first ice melting close to the eutectic temperatures of the H_2O-NaCl-$FeCl_2$ system (-37°C, Borisenko, 1977), the H_2O-$MgCl_2$ system (-35°C,

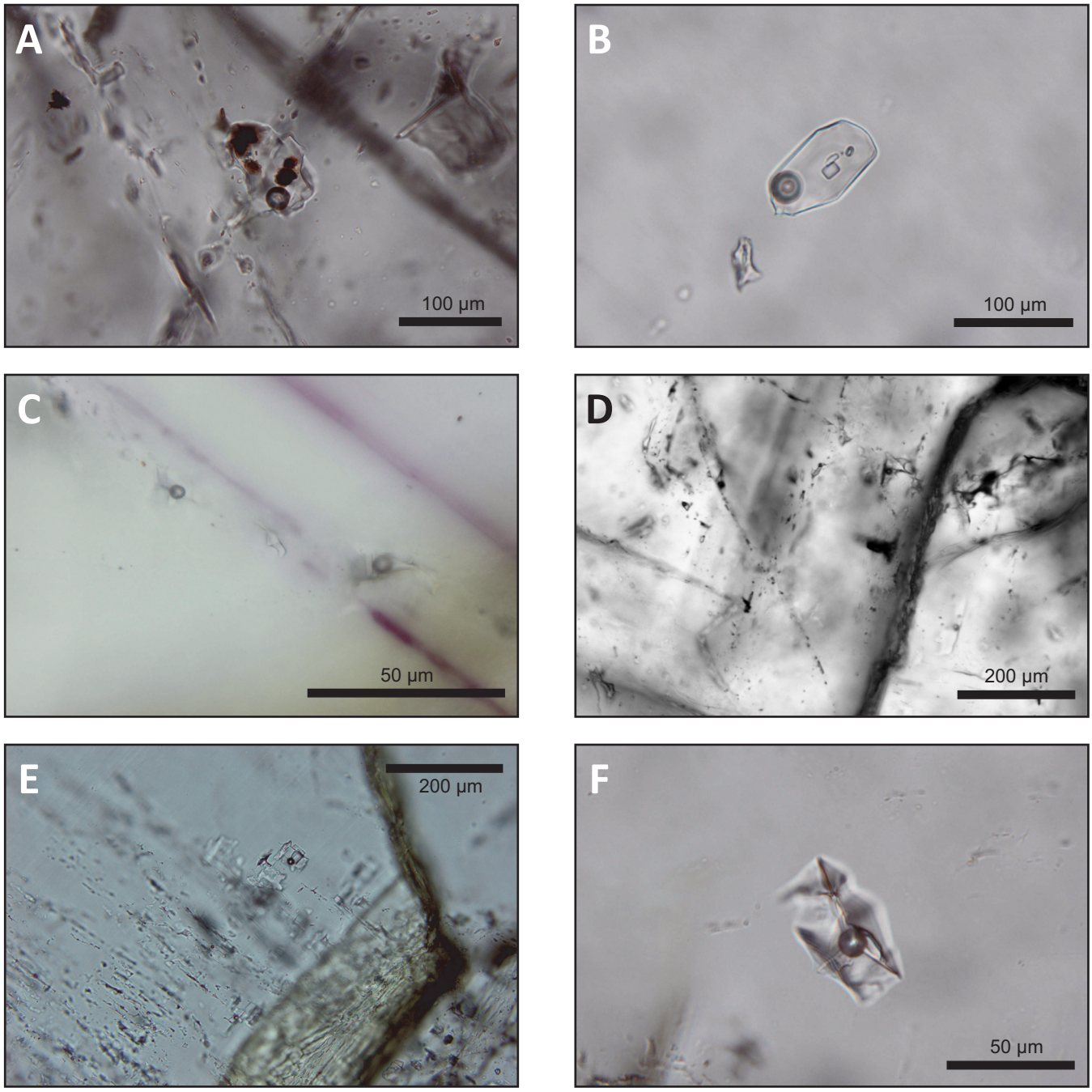

Plate 2. *Photomicrographs of fluorite-hosted fluid inclusions. A) Fluid inclusion with trapped hematite inclusion; B) Fluid inclusion with unidentified cubic solid inclusions; C) Trail of two-phase (L+V) Type-1 inclusions in purple fluorite (early-stage); D) Trail of secondary Type-2 inclusions crosscutting zoned yellow fluorite (early-stage); E) Two-phase Type-2 inclusions in reddish-grey fluorite (main-stage); F) Isolated two-phase Type-2 inclusion in late-stage blue fluorite.*

Dubois and Marignac, 1997) and the H_2O-NaCl-$MgCl_2$ system (-35.2°C, Spencer *et al.*, 1990; Table 2, Figure 9). The presence of salts other than NaCl and $CaCl_2$ is further suggested by complete freezing of Type-2 inclusions at temperatures above the eutectic temperature of the H_2O-NaCl-$CaCl_2$ system (-52°C) and clear melting of hydrohalite phases above the eutectic temperature of the H_2O-NaCl system (-20.8°C). Final ice melting temperatures for Type-2 inclusions range from -6.2 to -21.1°C, with most values above -11°C. These correspond to salinities of 9.5 to 23.1 eq. wt. % NaCl (Table 2, Figure 9). Total homogenization temperatures range from 98 to 183.1°C, with temperatures in indi-

Table 2. Summary of the microthermometric data from early-, main- and late-stage fluorite from the AGS Deposit

		Early		Main	Late
		Type 1	Type 2	Type 2	Type 2
n		63	55	76	58
Te	Average	-53.0	-40.4	-36.0	-40.0
	StDev	2.1	2.3	1.6	2.1
	Max	-48.6	-36.9	-33.1	-36.4
	Min	-55.9	-44.5	-38.6	-44.4
Tm (hh)	Average	-33.3	n/a	n/a	n/a
	StDev	4.8			
	Max	-24.2			
	Min	-41.2			
Tm (ice)	Average	-17.1	-8.9	-8.4	-7.8
	StDev	6.4	3.3	1.8	0.9
	Max	-6.3	-6.2	-6.6	-6.2
	Min	-28.2	-21.1	-12.8	-10.6
Salinity	Average	19.6	12.5	12.0	11.4
(eq. wt. %	StDev	5.4	3.1	2.0	1.0
NaCl)	Max	27.5	23.1	16.7	14.6
	Min	9.6	9.5	10.0	9.5
Salinity	Average	18.7	n/a	n/a	n/a
(eq. wt. %	StDev	4.7			
$NaCl+CaCl_2$)	Max	24.6			
	Min	10.2			
Molar	Average	0.25	n/a	n/a	n/a
Na/(Ca+Na)	StDev	0.15			
	Max	0.65			
	Min	0.10			
Th	Average	120.5	136.1	124.3	131.3
	StDev	19.7	12.8	10.6	12.8
	Max	159.6	160.8	143.4	183.1
	Min	89.3	109.6	98.0	101.8

vidual FIA varying by ± 5°C (Table 2, Figure 10). No significant variations were observed in the average homogenization temperatures of Type-2 inclusions in main-stage fluorites (124.3 ± 10.6°C) or late-stage (131.3 ± 12.8°C) fluorites. Two Type-2 inclusions hosted in green fluorite have anomalously high homogenization temperatures (379.5 and 426.4°C) but these temperatures are ~250–300°C higher than other inclusions in the same fluorite growth zones and indicate that these inclusions have undergone some form of post-entrapment modification (*e.g.*, leaking).

DISCUSSION

REE-Y AND TRACE ELEMENTS

The REE-Y patterns of fluorites are characterized by enrichment in HREE compared to LREE, reflected as a weak positive slope from La to Lu and the convex/concave nature of the LREE/HREE patterns (tetrad effect), and display a negative Eu anomaly and a positive Y anomaly (Figure 3). The positive slope from La to Lu observed in most phases is due to the increase in the formation constants of the fluoro complexes, which dominantly control the partitioning of elements in fluorite and are a function of the ionic radii that gradually increases from La to Lu (Bau and Dulski, 1995; Möller *et al.*, 1998 and references therein; van Hinsberg *et al.*, 2010). As a result, HREE form more stable complexes with F and are more likely than LREE to go into the F-rich fluid from the source granite. In addition, when fluorite precipitates from a given volume of solution, early fluorite is enriched in LREE and late fluorite is depleted in LREE. As the LREE-F complexes are less stable in the fluid than the HREE-F complexes, the LREE-F complexes will breakdown earlier than HREE-F complexes and LREE will preferentially go into the fluorite, which results in the fluid becoming richer in HREE. This causes REE-Y fractionation observed even within one phase (Figures 3 and 4). In addition, high flow rates produce fluorite with early fractionation pattern (enriched in LREE) and low flow rates produce fluorite with late fractionation pattern (depleted in LREE; Möller *et al.*, 1998), because influx of new fluids retains the initial LREE–HREE content of the fluid. Alternatively, the lack of new fluid influx will allow the fluid to become increasingly richer in HREE, which will result in fluorite also becoming increasingly richer in HREE as precipitation progresses. This may also account for some of the changes observed between the phases and even within one phase.

The tetrad effect displayed by the convex and concave shape of the REE-Y patterns was first described by Peppard *et al.* (1969; Figure 3). Such patterns are common in REE concentrations of hydrothermal minerals including fluorite, but also occur in altered granites (Zhenhua *et al.*, 2002; Azizi *et al.*, 2020). The possible reasons for the development of the tetrad effect include: 1) mineral fractionation in the source rocks, at separation from the source or during

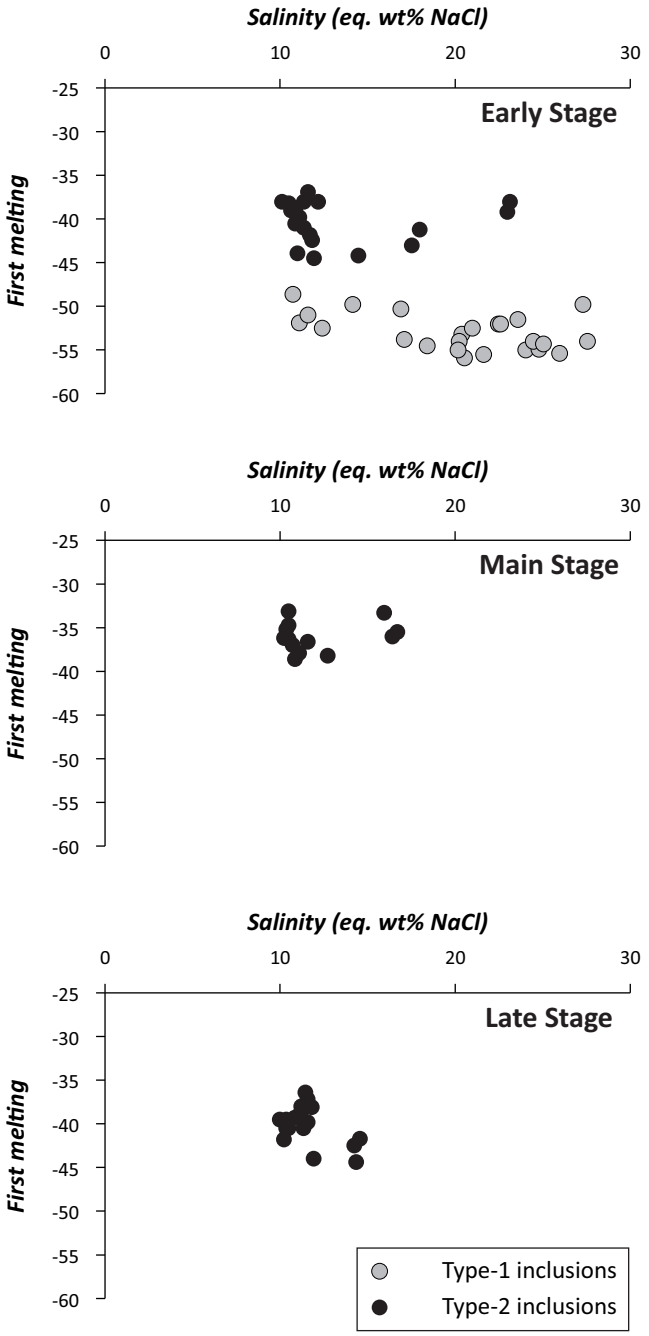

Figure 9. *Bivariate plots of salinity* vs. *first ice melting temperatures for Type-1 and Type-2 inclusions in early-, main- and late-stage fluorite.*

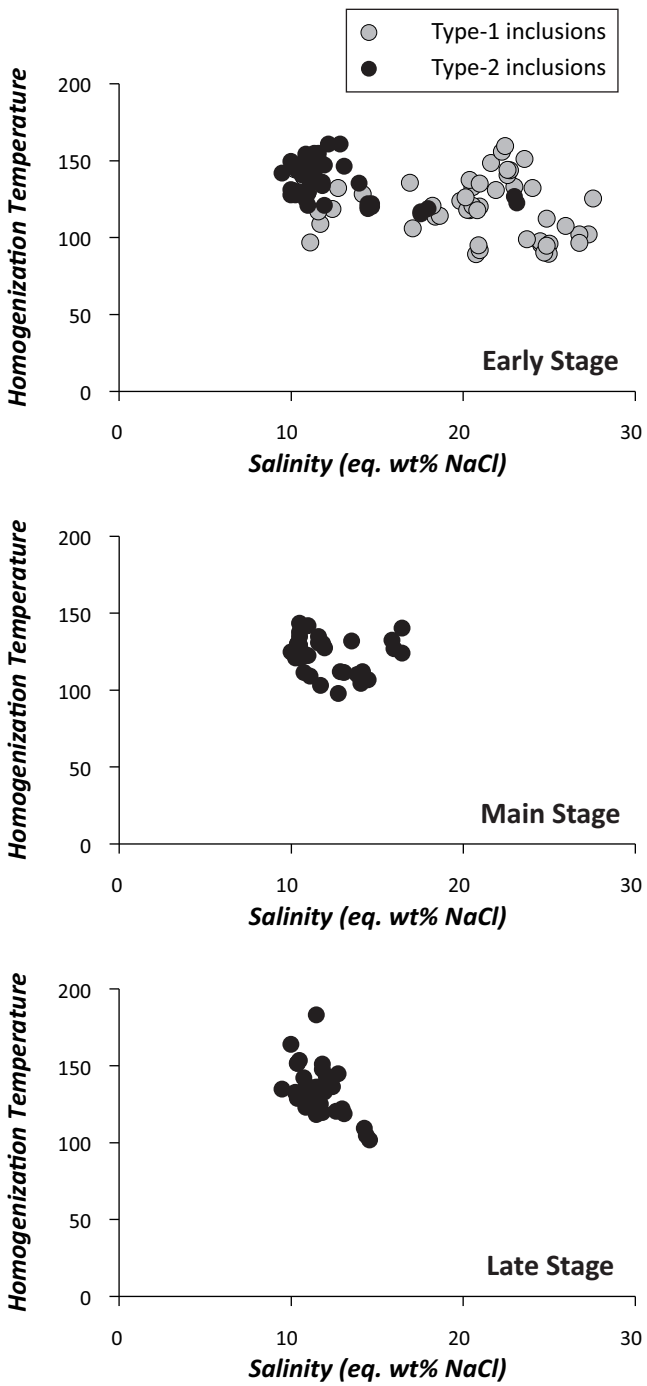

Figure 10. *Bivariate plots of salinity* vs. *homogenization temperatures for Type-1 and Type-2 inclusions in early-, main- and late-stage fluorite.*

migration of fluid; 2) F-complexation in fluid; 3) fluid-melt interaction; and 4) alteration (Azizi *et al.*, 2020 and references therein). In St. Lawrence, all of these processes likely occurred; therefore, it is difficult to determine the exact cause for the tetrad effect.

The negative Eu anomaly was most likely inherited from the granite, although it may have been modified by changes in redox conditions (Figures 3 and 5; Bau and Dulski, 1995; Möller *et al.*, 1998). The decrease in the size of the Eu anomaly in the last two phases indicates changes in the fluid composition, which is most likely due to prolonged interaction with the sedimentary rocks displaying a smaller Eu anomaly. Changes at the source granite or mix-

ing with other fluids may have also influenced the Eu anomalies.

The positive Y anomaly is a common feature of hydrothermal fluorites (Figures 3 and 6B, C; Bau and Dulski, 1995; Loges *et al.*, 2013). The lack of a significant Y anomaly in the granite and the sedimentary rocks suggests that the positive Y anomaly is not inherited from the host rocks. The ionic radii of Y and Ho are very similar and they are expected to behave similarly, but the Y/Ho ratios in hydrothermal fluorites range up to 200, which is significantly higher than chondrite values (27.7) and igneous rocks (up to 40; Bau and Dulski, 1995; Loges *et al.*, 2013). According to experimental studies, this is due to Y forming more stable di-fluoride complexes and REE, including Ho, forming less stable mono-fluoride complexes in F-rich fluids and the di-fluoride complexes having a greater affinity for the surfaces of the fluorite crystals during fluorite precipitation (Loges *et al.*, 2013). The stability of these complexes depends on the temperature and the F concentration, which is a function of the composition of the fluid. Bau and Dulski (1995) also observed the strong dependence of the Y anomaly on the composition of the fluid. The lack of a Y anomaly in calcite in the AGS deposit suggests that the Y anomaly was strongly dependent on the F concentration in the fluid, although the effect of small changes in temperature cannot be ruled out.

According to Bau and Dulski (1995), in a Y/Ho *vs.* La/Ho diagram co-genetic fluorites should display either similar Y/Ho and La/Ho ratios or a negative correlation between these ratios. A small range of Y/Ho and highly variable La/Ho ratios in co-genetic fluorites is interpreted to represent loss or gain of LREE after precipitation of the fluorite. However, as discussed earlier, LREE fractionation, represented by the La/Ho ratio, also occurs during precipitation of fluorite due to HREE forming more stable fluoro complexes and staying in the F-rich fluid (Möller *et al.*, 1998). Therefore, fluorites plotting along a line are considered part of one generation in this study. Based on the Y/Ho vs. La/Ho, the fluorites in the AGS deposit can be subdivided into four generations (Figure 6B). The first generation is represented by the earlier phases up to the grey fluorite, the second generation is represented by the grey fluorite, the third generation is represented by the green fluorite and the fourth generation is represented by the blue fluorite.

The Tb/Ca *vs.* Tb/La plot of the AGS fluorites suggest that all fluorites are hydrothermal and all phases, with the exception of the last phase (blue fluorite), are the result of primary crystallization (Figure 7). The last phase displays a line parallel to the secondary crystallization trend suggesting that this phase is the result of remobilization of earlier phases. The REE content of the last phase is generally lower, and the LREE content is significantly lower than the previous phases. This is consistent with the secondary nature of these fluorites due to the preferential remobilization of HREE by a F-rich fluid (Möller *et al.*, 1998).

The positive correlation of Na with the total REE-Y content observed in some phases suggests that the Ca^{2+} atom in the structure of fluorite is replaced by REE-Y^{3+}, with Na^{+} preserving neutrality in these phases (Figure 8A; Möller *et al.*, 1998). The slope of this correlation is variable for different phases, interpreted to be due to the presence of other elements with different charges, such as Al^{3+} or Zr^{4+}; indicative of changes in the composition of the fluids. This is in agreement with the presence of at least three generations of fluorite mineralization as indicated by the Y anomaly. The slope of the correlation in the blue fluorites appears to be the same as for the green fluorites, perhaps suggesting that the blue fluorites are formed *via* remobilization from the green fluorites. Sodium also has a positive correlation with Sr, which is expected as both Sr and Na substitute for Ca in the fluorite structure (Figure 8B).

The presence of Zr in some of the phases, and the lack of it in other phases, may indicate variable degrees of fluid/rock interaction (Figure 8C). The phases containing Zr typically form smaller veins indicating lower fluid/rock ratios whereas the phases with no Zr represent the main stage of mineralization and occur in extensional zones indicating higher fluid/rock ratio. Previous research in peralkaline intrusions suggest that Zr is remobilized at low temperatures forming F complexes in acidic fluids with pH <2 in fluids containing both F and Cl (Gysi and Williams-Jones, 2013).

FLUIDS ASSOCIATED WITH THE FORMATION OF THE AGS FLUORITE DEPOSIT

Fluid inclusion analysis indicate that at least two main fluid types were associated with fluorite precipitation in the AGS fluorite deposit. Early-stage fluorites (purple, yellow and hematitic fluorite) precipitated from low temperature (average Th 120.5 ± 19.7°C), and moderate to high salinity (9.6 to 27.5 eq. wt. % NaCl) H_2O-NaCl-$CaCl_2$ fluids (Table 2, Figures 9 and 10). The wide range of salinities and Na/(Na + Ca) ratios observed in these inclusions indicate that fluorite precipitated due to the mixing of two or more fluids. When plotted on a ternary H_2O-NaCl-$CaCl_2$ diagram, two mixing trends are observed (Figure 11): 1) a fluorine-rich high salinity H_2O-$CaCl_2$ fluid of possible magmatic origin mixing with a low salinity NaCl dominated fluid (meteoric), and 2) a fluorine-rich high salinity H_2O-$CaCl_2$ fluid of possible magmatic origin mixing with high salinity H_2O-NaCl-$CaCl_2$ fluid (basinal brine) in the yellow fluorites.

Precipitation of main-stage and late-stage fluorites occurred over similar temperatures as the early-stage fluo-

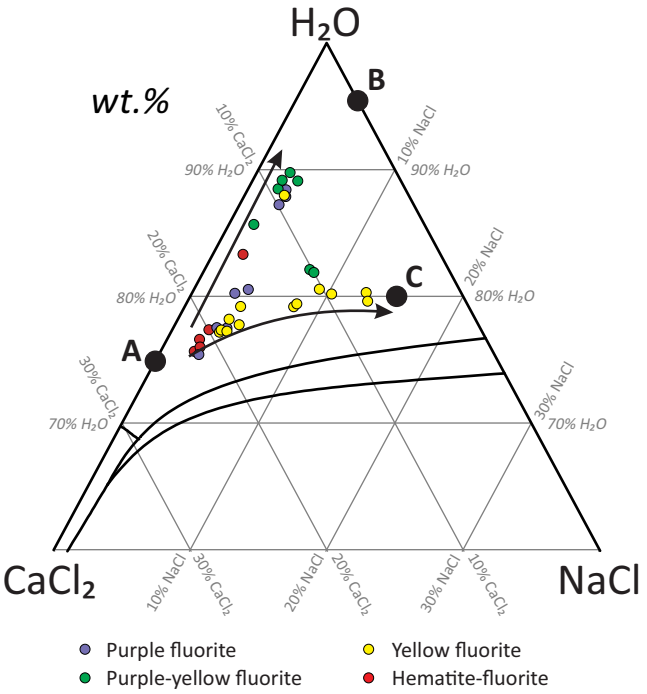

Figure 11. *Ternary H_2O-NaCl-$CaCl_2$ plot (wt. %), with fluid compositions calculated using Tm (hh) and Tm (ice) and the spreadsheet provided by Steele-MacInnis* et al. *(2011). Also included are hypothetical fluid compositions for a high salinity Ca-rich magmatic fluid (A), low salinity meteoric fluid (B) and high salinity basinal brine (C).*

rites (average Th 124.3 ± 10.6° and 131.3 ± 12.8°C, respectively). However, fluid inclusion data indicate a marked change in fluid composition (Table 2, Figures 9 and 10). In comparison to Type-1 inclusions, Type-2 inclusions in the main-stage and late-stage fluorites have a much narrower range of salinities (9.5 to 16.7 eq. wt. % NaCl), and first ice melting temperatures indicate that these fluids contain salts such as $MgCl_2$ and $FeCl_2$, in addition to NaCl and $CaCl_2$. The narrow range of salinities, and the relatively consistent fluid compositions, indicate that fluid mixing was not an important process in the precipitation of these fluorites. Fluorite precipitation instead is interpreted to have been associated with the reactivity of acidic hydrothermal fluids with sedimentary rocks and associated changes in pH.

Strong *et al.* (1984) reported fluid inclusion data from a series of granite-hosted fluorite veins in the area. In contrast to the results of this study, Strong *et al.* (1984) recorded a wide range of homogenization temperatures (100 to 450°C) and suggested that fluorite precipitation was controlled by pH changes during fluid boiling. Collins (1992) presented a more detailed fluid inclusion study of granite-hosted fluorite veins as well as the Grebe's Nest occurrence in the western end of the AGS deposit. He also reported a wide range of homogenization temperatures (50 to 500°C), but with a pronounced maximum homogenization temperature at ~100°C (90% of inclusions with Th of 70 to 140°C) and no evidence of boiling. This is consistent with the results of this study, which find no evidence of fluid boiling during the formation of the AGS deposit. The higher homogenization temperatures recorded by Collins (1992) may be related to post-entrapment modification as has been suggested for anomalously high homogenization temperatures recorded during this study. Collins (1992) also recorded a strong bimodal salinity distribution (at ~12 and 25 eq. wt. % NaCl) and eutectic temperatures over similar ranges to those recorded from Type-1 and Type-2 inclusions. This suggests that the fluids associated with the formation of the AGS deposit were analogous to those responsible for mineralization hosted within the SLG. Although no evidence of fluid boiling has been identified during this study, further work is required to determine the importance of fluid boiling during the earlier magmatic stages of fluid evolution in the SLG as suggested by Strong *et al.* (1984).

AGS FLUORITE MINERALIZATION

Early Stage

The early stage of fluorite mineralization consists of breccias with clasts of host rocks in a fluorite matrix and relatively small veins, indicating a low fluid/rock ratio (Plate 1A). The fluid inclusion analysis indicates that fluorite precipitated due to mixing of a high-salinity H_2O-NaCl-$CaCl_2$ magmatic fluid with a low-salinity meteoric water and, in the yellow fluorites, with a high-salinity basinal brine (H_2O-NaCl-$CaCl_2$; Figure 11). The fluids were oxidizing, suggested by the presence of hematite with fluorites in this stage. They were also acidic, suggested by the presence of sericite as the main alteration mineral around the veins. There is no major change in the REE-Y patterns of the fluorites. The size of the Eu anomaly indicates the strong influence of the granite and is consistent with the presence of a magmatic fluid (Figures 3 and 5). The fluorites plot along the primary crystallization trend (Figure 7). The consistent size of the Y anomaly, and same slope of correlation between Na and the total REE-Y content, indicate that there were no major changes in the composition of the fluids, which is in agreement with the fluid inclusion analysis (Figures 6B and 8A).

Fluorite mineralization was initiated by the intrusion of the granite and volatile exsolution from the cooling granite. The REE-Y patterns of early fluorites are consistent with their origin from volatiles exsolving from the cooling granite (Magotra *et al.*, 2017). The enrichment in HREE is due to the F forming more stable complexes with HREE and preferentially removing the HREE from the granite as a result in the derived fluids (*e.g.*, Möller *et al.*, 1998). In

addition, the similarities in the size of the negative Eu anomalies suggest that the Eu anomaly was most likely inherited from the granite. The Y anomaly is specific to fluorite and is controlled by complexation in the fluids.

Main Stage

The main stage of fluorite mineralization consists of massive reddish-grey and grey fluorites separated by a band of sulphides composed of sphalerite and galena (Plate 1B). This stage, formed in extensional zones, developed through continuous movement along the strike-slip fault (Magyarosi *et al.*, 2019b), indicative of high fluid/rock ratio. Fluid inclusion analysis indicates a change in the composition of the fluids compared to those associated with the early-stage mineralization (Table 2, Figures 9 and 10). In addition to NaCl and $CaCl_2$, the ice melting temperatures of the fluids indicate the presence of other salts such $MgCl_2$ and/or $FeCl_2$. The narrow range of salinities suggest that fluorite precipitation was not controlled by fluid mixing, but more likely was associated with other changes such as pH. The reddish-grey fluorites indicate the presence of fine-grained hematite in the fluorite, suggesting that the fluids were still oxidizing. However, the presence of sulphides, and the lack of hematite, in the grey fluorites suggest a change in the O and S fugacities.

Despite the changes in the fluids indicated by the fluid inclusion analysis, the REE-Y patterns of the reddish-grey fluorites are similar in every way to the early-stage fluorites (Figure 3). Their HREE and LREE contents are in the same range and they display the same size of Eu and Y anomalies, and the same slope of correlation between Na and the total REE-Y content (Figures 4, 5 and 6B, C). This suggests that at the beginning of the main stage, the changes in the fluids did not affect the REE-Y contents of the fluorites.

The grey fluorites still plot along the primary crystallization trend, but they are characterized by a significant increase (~10-fold) in the HREE content compared to the earlier phases (Figures 3 and 4). The size of the Eu anomaly does not change, but the size of the Y anomaly slightly decreases, suggesting a change in the F concentration of the fluid (Figures 5 and 6B, C; Loges *et al.*, 2013). The slope of the correlation between Na and total REE-Y content also displays significant changes, suggesting a change in the composition of the fluids (Figure 8A). The nature of the fluid inclusions did not change between the reddish-grey and grey fluorites, but there was clearly a change in the fluids, not detected by fluid inclusion analysis, that included changes in the O and S fugacities.

The changes between the early and main stages of mineralization are most likely caused by the development of local extensional zones in the veins, which allowed larger amounts of magmatic fluid from the underlying granite and meteoric water/basinal fluids from other sources to enter the veins. This event represents the peak of the hydrothermal activity and it enhanced the circulation of the fluids in the overlying sedimentary rocks. This was a combined effect of more intense brecciation of the overlying sedimentary rocks and the increased amounts of fluids. The changes observed between the two phases in the main stage are the result of prolonged circulation of fluids interacting with the sedimentary rocks.

Late Stage

The late stage of fluorite mineralization consists of green and blue fluorites forming both on top of earlier phases, as well as in new smaller veins developed during continuous movement along the strike-slip fault represented by new R shears (Plate 2C; Magyarosi *et al.*, 2019b). This indicates a decrease in the fluid/rock ratio from the main stage. The green fluorites are locally associated with abundant calcite, suggesting the presence of carbonates in the fluids. Fluid inclusion analysis shows no major changes in the temperature, salinity and composition of the fluids from the main stage.

There are major changes in the REE-Y patterns of fluorites in this stage. The green fluorites are characterized by the lack of fractionation between HREE and LREE, change in the slope of positive correlation between Na and total REE-Y content, a smaller Eu anomaly and a larger Y anomaly than fluorites in previous stages (Figures 3–7 and 9). Green fluorites still plot parallel to the primary crystallization trend (Figure 8). The smaller Eu anomaly probably indicates a larger influence of the sedimentary rocks on the REE-Y composition of fluorites. The change in the slope of the positive correlation between Na and total REE-Y, and in the size of the Y anomaly, suggest changes in the composition of the fluids, including the F concentration.

The blue fluorites are characterized by a significant decrease in both LREE and HREE contents and the reappearance of the HREE enrichment relative to the LREE (Figures 3 and 4). There is a further decrease in the size of the Eu anomaly, suggesting an even stronger influence of the sedimentary rocks (Figure 5). The slope of the correlation between Na and total REE-Y is similar, but not as well defined due to the low REE-Y contents (Figure 8A). The blue fluorites plot along the secondary crystallization trend indicating that they formed due to remobilization of earlier phases, most likely the green fluorites as suggested by the similarities between their REE-Y signatures (Figure 7). The reappearance of the HREE *vs.* LREE fractionation is in agreement with the remobilized origin of the blue fluorites,

because HREE would preferentially enter a F-rich fluid (Möller *et al.*, 1998).

The two major changes associated with the late stage of mineralization include the increased influence of the sedimentary rocks and the addition of carbonates to the fluids. The larger influence of the sedimentary rocks was due to the decrease in the fluid/rock ratio with the fluid buffered increasingly by the sedimentary rocks. Further cooling of the granite caused the hydrothermal activity to wane, and resulted in smaller veins in the late stage. Prolonged circulation of the fluids in the overlying sedimentary rocks with smaller fluid/rock ratio resulted in the larger influence of the sedimentary rocks in the REE-Y signatures of fluorites.

Peralkaline granites are typically associated with a carbon phase that initially occurs as hydrocarbons, but with cooling, it becomes increasingly oxidized and acidic and changes to CO_2 (Salvi and Williams-Jones, 2006; Gysi and Williams-Jones, 2013; Dostal *et al.*, 2014; Gysi *et al.*, 2016; Vasyukova *et al.*, 2016; Vasyukova and Williams-Jones, 2018; Ducharme, 2019). With further cooling, carbonate becomes the major carbon phase in the fluids, and reacting with Ca forms calcite. Calcite also occurs in the granite as a late alteration, consistent with the late nature of calcite in the veins. The last change in the veins was the remobilization of earlier fluorites, mostly green fluorites, to form the blue fluorites.

CONCLUSIONS

Trace-element contents, including REE and Y, in conjunction with fluid inclusion analysis were used to record the evolution of the AGS fluorite deposit. These methods, combined with detailed field and petrographic observations, provide an excellent tool to detect changes in the fluorites in different stages of mineralization and indicate possible causes for these changes.

Fluorite mineralization in the AGS area was initiated during the intrusion of a main granitic phase of the SLG underlying the sedimentary rocks, with exsolution of volatiles from the cooling granite. The early stage of fluorite mineralization is characterized by smaller veins and breccias suggesting a low fluid/rock ratio. Fluid inclusion analysis indicate fluids composed of H_2O-NaCl-$CaCl_2$ and mixing of a magmatic fluid with meteoric water and a basinal brine. Fluorite precipitation was most likely due to mixing of the fluids. The fluids were oxidizing and acidic. Fluorites in this stage share very similar REE-Y patterns, with an enrichment of HREE relative to LREE, a negative Eu anomaly inherited from the granite, and a positive Y anomaly. This pattern is consistent with the fluorites originating from volatile exsolution from the cooling granite.

The main stage represents the peak of hydrothermal activity, as indicated by the veins opening up resulting in a high fluid/rock ratio. The salinity of the fluids changed to moderate, and the fluid contained salts, such as $MgCl_2$ and/or $FeCl_2$ in addition to NaCl and $CaCl_2$. Fluorite precipitation was not due to mixing of fluids, but rather was more likely related to changes in pH. Initially, in the reddish-grey fluorites, there is no change in the REE-Y pattern from the early-stage fluorites. The REE-Y patterns change significantly in the grey fluorites, illustrated as a 10-fold increase in the HREE content and a slight decrease in the size of the Y anomaly, both indicating a change in the F concentration of the fluids, which is coupled with changes in O and S fugacities. These changes are interpreted to be due to prolonged fluid/rock interaction with the fluids being increasingly buffered by the sedimentary rocks.

The last stage of fluorite mineralization represents the waning stage of the hydrothermal activity. Fluorite mineralization occurs in smaller veins and in small open spaces on top of earlier fluorites, suggesting a lower fluid/rock ratio. Fluid inclusion analysis shows no changes in the fluids from the main stage, but REE-Y patterns change significantly in this stage. The size of Eu anomaly gradually decreases, and the size of Y anomaly slightly increases. The REE-Y pattern of the green fluorites is flat, showing no enrichment in HREE compared to LREE. The last phase of mineralization, represented by the blue fluorites, is characterized by a significant decrease in the total REE-Y content, and the reappearance of the HREE enrichment. These changes are due to the fluids being increasingly buffered by the sedimentary rocks and the addition of carbonates to the fluids. The last phase is the result of remobilization of earlier phases, probably mostly green fluorites.

ACKNOWLEDGMENTS

We would like to thank Melissa Mills and Alex Bugden, student assistants, for their help during fieldwork. We are grateful to Chris Finch for the whole-rock analysis, Joanne Rooney for typesetting, John Hinchey for all his support, Andrea Mills and Hamish Sandeman for the discussions and encouragement. Gerry Hickey helped with providing equipment and ensuring our safety in the field. Nick Pochereva is thanked for preparing the samples for the SIMS and LA-ICP-MS analysis, Graham Layne and Glenn Piercey are thanked for the SIMS analysis and Markus Wälle is thanked for the LA-ICP-MS analysis. We are grateful to Mellissa Lambert, Greg Pittman, Daron Slaney and the surveyors from Canada Fluorspar Inc. who were extremely helpful during fieldwork in the mine area.

REFERENCES

Azizi, M.R., Abedini, A. and Alipour, S.
2020: Application of lanthanides tetrad effect as a geochemical indicator to identify fluorite generations: A case study from the Laal-Kan fluorite deposit, NW Iran. Comptes Rendus Géoscience – Sciences de la Planète, Volume 352, Issue 1, pages 43-58.

Bakker, R.J. and Baumgartner, M.
2012: Unexpected phase assemblages in inclusions with ternary H_2O-salt fluids at low temperatures. Central European Journal of Geosciences, Volume 4, pages 225-237.

Bau, M. and Dulski, P
1995: Comparative study of yttrium and rare-earth element behaviours in fluorine-rich hydrothermal fluids. Contributions to Mineralogy and Petrology, Volume 119, pages 213-223.

Bodnar, R.J.
1993: Revised equation and table for determining the freezing point depression of H_2O-NaCl solutions. Geochimica et Cosmochimica Acta, Volume 57, pages 683-684.

Borisenko, A.S.
1977: Study of the salt compositions of solutions of gas-liquid inclusions in minerals by the cryometric method. Geologiya i Geofizika, Volume 18, pages 16-27.

Collins, C.J.
1992: A fluid inclusion and trace element geochemical study of the granite-hosted, St. Lawrence fluorspar deposits and related host rocks. M.Sc. Thesis, Memorial University of Newfoundland, St. John's.

Coşanay, P., Kirat, E., Çevik, N., Kizilkanat, C., Mutlu, H. and Koç, Ş.
2017: Geochemical, microthermometric, and isotopic constraints on the origin of fluorite deposits in central Anatolia, Turkey. Turkish Journal of Earth Sciences, Volume 26, pages 1-21.

Deng, X., Chen, Y., Yao, J. Bagas, L. and Tang, H.
2014: Fluorite REE-Y (REY) geochemistry of the *ca.* 850 Ma Tumen molybdenite–fluorite deposit, eastern Qinling, China: Constraints on ore genesis. Ore Geology Reviews, Volume 63, pages 532-543.

Dostal, J., Kontak, D.J. and Karl, S.M.
2014: The Early Jurassic Bokan Mountain peralkaline granitic complex (southeastern Alaska): Geochemistry, petrogenesis and rare-metal mineralization. Lithos, Volumes 202-203, pages 395-412.

Dubois, M. and Marignac, C.
1997: The H_2O-NaCl-$MgCl_2$ ternary phase diagram with special application to fluid inclusion studies. Economic Geology, Volume 92, pages 114-119.

Ducharme, T.A.
2019: Petrogenesis, emplacement setting, and magmatic-hydrothermal mineralization of the peralkaline Flowers River Igneous Suite, Hopedale Block, Labrador. Department of Earth Sciences, University of New Brunswick, Fredericton, NB, Unpublished M.Sc. Thesis, 156 pages.

Finch, C., Roldan, R., Walsh, L., Kelly, J. and Amor, S.
2018: Analytical methods for chemical analysis of geological materials. Government of Newfoundland and Labrador, Department of Natural Resources, Geological Survey, Open File NFLD/3316, 67 pages.

Gagnon, J.E., Samson, I.M., Fryer, B.J. and Williams-Jones, A.E.
2003: Compositional heterogeneity in fluorite and the genesis of fluorite deposits: insights from LA-ICP-MS analysis. The Canadian Mineralogist, Volume 41, pages 365-382.

Goldstein R.H.
2003: Petrographic analysis of fluid inclusions. *In* Short Course Series. *Edited by* I. Samson, A. Anderson and D. Marshall. Mineralogical Association of Canada, Volume 32, pages 9-53.

Goldstein R.H. and Reynolds T.J.
1994: Systematics of fluid inclusions in diagenetic minerals. SEPM Short Course Notes, Volume 31, 188 pages.

Gysi, A.P. and Williams-Jones, A.E.
2013: Hydrothermal mobilization of pegmatite-hosted REE and Zr at Strange Lake, Canada: A reaction path model. Geochimica et Cosmochimica Acta, Volume 122, pages 324-352.

Gysi, A.P., Williams-Jones, A.E. and Collins, P.
2016: Lithogeochemical vectors for hydrothermal processes in the Strange Lake peralkaline granitic REE-Zr-Nb deposit. Economic Geology, Volume 111, pages 1241-1276.

Haschke, S., Gtzmer, J., Wohlgemuth-Ueberwasser, C.C., Kraemer, D. and Burisch, M.
2021: The Niederschlag fluorite-(barite) deposit, Erzgebirge/Germany–a fluid inclusion and trace element study. Mineralium Deposita, accepted manuscript.

Hiscott, R.
1981: Stratigraphy and sedimentology of the Rock Harbour Group, Flat Islands, Placentia Bay, Newfoundland Avalon Zone. Canadian Journal of Earth Sciences, Volume 18, pages 495-508.

Kerr, A., Dickson, W.L., Hayes, J.P. and Fryer, B.J.
1993a: Devonian postorogenic granites on the southeastern margin of the Newfoundland Appalachians: A review of geology, geochemistry, petrogenesis and mineral potential. *In* Current Research. Government of Newfoundland and Labrador, Department of Mines and Energy, Geological Survey Branch, Report 93-1, pages 239-278.

Kerr, A., Dunning, G.R. and Tucker, R.D.
1993b: The youngest Paleozoic plutonism of the Newfoundland Appalachians: U–Pb ages from the St. Lawrence and François granites. Canadian Journal of Earth Sciences, Volume 30, pages 2328-2333.

King A.F.
1988: Geology of the Avalon Peninsula, Newfoundland (parts of 1K, 1L, 1M, 1N and 2C). Government of Newfoundland and Labrador, Department of Mines and Energy, Mineral Development Division, Map 88-01.

Krogh T.E., Strong D.F., O'Brien, S.J. and Papezik V.S.
1988: Precise U-Pb zircon dates from the Avalon Terrane in Newfoundland: Canadian Journal of Earth Sciences, Volume 25, pages 442-453.

Lilly, H.D.
1966: Late Precambrian and Appalachian tectonics in the light of submarine exploration on the Great Bank of Newfoundland and in the Gulf of Saint Lawrence; Preliminary views. American Journal of Science, Volume 264, pages 569-574.

Loges, A., Migdisov, A.A., Wagner, T., Williams-Jones, A.E. and Markl, G.
2013: An experimental study of the aqueous solubility and speciation of Y(III) fluoride at temperatures up to 250°C. Geochimica et Cosmochimica Acta, Volume 123, pages 403-415.

Magotra, R., Namga, S., Singh, P., Arora, N. and Srivastava, P.K.
2017: A new classification scheme of fluorite deposits. International Journal of Geoscience, Volume 8, pages 599-610.

Magyarosi, Z., Pochereva, N. and Layne, G.
2019a: Database of fluorite mineralization and of the host rocks in the St. Lawrence area, Burin Peninsula (NTS map sheets 01L/13, 14 and 01M/03). Government of Newfoundland and Labrador, Department of Natural Resources, Geological Survey, Open File NFLD/3381, 11 pages.

Magyarosi, Z., Sparkes, B.A., Conliffe, J. and Dunning, G.R.
2019b: The AGS fluorite deposit, St. Lawrence: paragenetic sequence, fluid inclusion analysis, structural control, host rock geochronology and implications for ore genesis. *In* Current Research. Government of Newfoundland and Labrador, Department of Natural Resources, Geological Survey, Report 19-1, pages 59-83.

McDonough, W.F. and Sun, S.S.
1995: The composition of the Earth. Chemical Geology, Volume 120, pages 223-253.

Mills, A.J., Calon, T. and Peddle, C.
2016: Preliminary investigations into the structural geology of the Bonavista Peninsula, northeast Newfoundland. *In* Current Research. Government of Newfoundland and Labrador, Department of Natural Resources, Geological Survey, Report 16-1, pages 133-152.

Mills, A.J., Dunning, G.R., Murphy, M. and Langille, A.
2017: New geochronological constraints on the timing of magmatism for the Bull Arm Formation, Musgravetown Group, Avalon Terrane, northeastern Newfoundland. *In* Current Research. Government of Newfoundland and Labrador, Department of Natural Resources, Geological Survey, Report 17-1, pages 1-17.

Möller, P., Bau, M., Dulski, P. and Lüders, V.
1998: REE and yttrium fractionation in fluorite and their bearing on fluorite formation. Proceedings of the Ninth Quadrennial IAGOD Symposium. *Edited by* Richard D. Hagni. International Association on the Genesis of Ore Deposits, IAGOD, pages 575-592.

Möller, P., Parekh, P.P. and Schneider, H.-J.
1976: The application of Tb/Ca-Tb/La abundance ratios to problems of fluorspar genesis. Mineralium Deposita, Volume 11, pages 111-116.

Murphy, J.B., McCausland, P.J.A., O'Brien, S.J., Pisarevsky, S. and Hamilton, M.A.
2008: Age, geochemistry and Sm-Nd isotopic signature of the 0.76 Ga Burin Group: Compositional equivalent of Avalonian basement? Precambrian Research, Volume 165, pages 37-48.

Myrow, P.M.
1995: Neoproterozoic rocks of the Newfoundland Avalon Zone. Precambrian Research, Volume 73, pages 123-136.

O'Brien, S.J., Dunning, G.R., Knight, I. and Dec, T.
1989: Late Precambrian geology of the north shore of Bonavista Bay (Clode Sound to Lockers Bay). *In* Report of Activities. Government of Newfoundland and Labrador, Department of Mines and Energy, Geological Survey Branch, pages 49-50.

O'Brien, S.J., O'Brien, B.H., Dunning, G.R. and Tucker, R.D.
1996: Late Neoproterozoic Avalonian and related peri-Gondwanan rocks of the Newfoundland Appalachians. Geological Society of American, Special Paper 304, pages 9-28.

O'Brien, S.J.F., Strong, D.F., Strong, P., Taylor, S.W. and Wilton, D.H.
1976: Geology of the Marystown–St. Lawrence area. *In* Report of Activities, 1975. Government of Newfoundland and Labrador, Department of Mines and Energy, Mineral Development Division, Report 76-1.

O'Driscoll, C.F., Dean, M.T., Wilton, D.H.C. and Hinchey, J.G.
2001: The Burin Group: A late Proterozoic ophiolite containing shear-zone hosted mesothermal-style gold mineralization in the Avalon Zone, Burin Peninsula, Newfoundland. *In* Current Research. Government of Newfoundland and Labrador, Department of Mines and Energy, Grological Survey, Report 01-1, pages 229-246.

Papezik, V.S.
1974: Igneous rocks of the Avalon Platform. Geological Association of Canada, Annual Fieldtrip Manual B-5, 22 pages.

Peppard, D.F., Mason, G.W. and Lewey, S.
1969: A tetrad effect in the liquid-liquid extraction ordering of lanthanides (III). Journal of Inorganic Nuclear Chemistry, Volume 31, pages 2271-2272.

Pochereva, N.
2019: REE and Pb Isotope Systematics of the AGS Deposit and Other Fluorite Ores Associated with the St. Lawrence Granite. Unpublished B.Sc. thesis. Memorial University of Newfoundland, St. John's, NL, 103 pages.

Reeves, J.H., Sparkes, B.A. and Wilson, N.
2016: Paragenesis of fluorspar deposits on the southern Burin Peninsula, Newfoundland, Canada. Canadian Institute of Mining Journal, Volume 7, Number 2, pages 77-86.

Salvi, S. and Williams-Jones, A.E.
2006: Alteration, HFSE mineralisation and hydrocarbon formation in peralkaline igneous systems: Insights from the Strange Lake Pluton, Canada. Lithos, Volume 91, pages 19-34.

Schlegel, T.U., Wagner, T. and Fusswinkel, T.
2020: Fluorite as indicator mineral in iron oxide-copper-gold systems: explaining the IOCG deposit diversity. Chemical Geology, Volume 548, pages 1-9.

Schwinn, G. and Markl, G.
2005: REE systematics in hydrothermal fluorite. Chemical Geology, Volume 216, pages 225-248.

Shepherd, T.J., Rankin, A.H. and Alderton, D.H.M.
1985: A practical guide to fluid inclusions, Blackie, London, 239 pages.

Skehan, J.W.
1997: Assembly and dispersal of supercontinents: The view from Avalon. Journal of Geodynamics, Volume 23, pages 237-262.

Smith, S.A. and Hiscott, R.N.
1984: Latest Precambrian to Early Cambrian basin evolution, Fortune Bay, Newfoundland: Fault-bounded basin to platform. Canadian Journal of Earth Sciences, Volume 21, pages 1379-1392.

Sparkes, B.A. and Reeves, J.R.
2015: AGS Project, project review and resource estimate, Canada Fluorspar Inc. Presentation, Baie Verte Mining Conference.

Sparkes, G.W. and Dunning, G.R.
2014: Late Neoproterozoic epithermal alteration and mineralization in the western Avalon Zone: A summary

of mineralogical investigations and new U/Pb geochronological results. *In* Current Research. Government of Newfoundland and Labrador, Department of Natural Resources, Geological Survey, Report 14-1, pages 99-128.

Spencer, R.J., Møller, N. and Weare, J.H.
1990: The prediction of mineral solubilities in natural waters: a chemical equilibrium model for the Na-K-Ca-Mg-Cl-SO_4-H_2O system at temperatures below 25°C. Geochimica et Cosmochimica Acta, Volume 54, pages 575-590.

Steele-MacInnes M., Bodnar R.J. and Naden J.
2011: Numerical model to determine the composition of H_2O-NaCl-$CaCl_2$ fluid inclusions based on microthermometric and microanalytical data. Geochimica et Cosmochimica Acta, Volume 75, pages 21-40.

Strong, D.F., Fryer, B.J. and Kerrich, R.
1984: Genesis of the St. Lawrence fluorspar deposits as indicated by fluid inclusion, rare earth element, and isotopic data. Economic Geology, Volume 79, pages 1142-1158.

Strong, D.F., O'Brien, S.J., Strong, P.G., Taylor, S.W. and Wilton, D.H.
1976: Geology of the St. Lawrence and Marystown map sheets (1L/14, 1M/3), Newfoundland, Preliminary report for Open File release, NFLD 895, 44 pages.

1978: Geology of the Marystown (1M/13) and St. Lawrence (1L/14) map areas, Newfoundland. Government of Newfoundland and Labrador, Department of Mines and Energy, Mineral Development Division, Report 78-7, 81 pages.

Van Alstine, R.E.
1948: Geology and mineral deposits of the St. Lawrence area, Burin Peninsula, Newfoundland. Newfoundland Geological Survey, Bulletin Number 23, 73 pages.

van Hinsberg, V.J., Migdisov, A.A. and Williams-Jones, A.E.
2010: Reading the mineral record of fluid composition from element partitioning. Geology, Volume 38, pages 847-850.

van Staal, C. and Zagorevski, A.
2017: Accreted terranes of the Appalachian Orogen in central Newfoundland. Geological Association of Canada – Mineralogical Association of Canada, Field Trip Guidebook, 114 pages.

Vasyukova, O.E. and Williams-Jones, A.E.
2018: Direct measurement of metal concentrations in fluid inclusions, a tale of hydrothermal alteration and REE ore formation from Strange Lake, Canada. Chemical Geology, Volume 483, pages 385-396.

Vasyukova, O.E., Williams-Jones, A.E. and Blamey, N.J.F.
2016: Fluid evolution in the Strange Lake granitic pluton, Canada: Implications for HFSE mobilization. Chemical Geology, Volume 444, pages 83-100.

Williams, H.
1995: Geology of the Appalachian-Caledonian Orogen in Canada and Greenland. Geological Survey of Canada, Geology of Canada, No. 6 (also Geological Society of America, The Geology of North America, Volume F1).

Williams, H., Kennedy, M.J. and Neal, E.R.W.
1974: The northeastward termination of the Appalachian Orogen. *In* Ocean Basins and Margins, Volume 2. *Edited by* A.E.M. Nairn and F.G. Stehli. Plenum Press, New York, pages 79-123.

Zhenhua, Z., Xiaolin, X., Xiaodong, H., Yixian, W., Qiang, W., Zhiwei, B. and Jahn, B.
2002: Controls on the REE tetrad effect in granites: Evidence from the Qianlishan and Baerzhe Granites, China. Geochemical Journal, Volume 36, pages 527-543.